Mon. Not. R. Astron. Soc. **398,** 321–332 (2009) doi:10.1111/j.1365-2966.2009.15150.x

Large-scale non-Gaussian mass function and halo bias: tests on *N*-body simulations

M. Grossi,[1⋆] L. Verde,[2,3⋆] C. Carbone,[3⋆] K. Dolag,[1⋆] E. Branchini,[4⋆] F. Iannuzzi,[1,5⋆] S. Matarrese[6⋆] and L. Moscardini[5,7⋆]

[1]*Max-Planck-Institut fuer Astrophysik, Karl-Schwarzschild Strasse 1, D-85748 Garching, Germany*
[2]*ICREA (Institució Catalana de Recerca i Estudis Avançats)*
[3]*Institute of Space Sciences (CSIC–IEEC), UAB, Barcelona 08193, Spain*
[4]*Dipartimento di Fisica, Università di Roma TRE, via della Vasca Navale 84, I-00146 Roma, Italy*
[5]*Dipartimento di Astronomia, Università di Bologna, via Ranzani 1, I-40127 Bologna, Italy*
[6]*Dipartimento di Fisica 'G. Galilei', Università degli Studi di Padova and INFN Sezione di Padova, via Marzolo 8, I-35131 Padova, Italy*
[7]*INFN, Sezione di Bologna, viale Berti Pichat 6/2, I-40127 Bologna, Italy*

Accepted 2009 May 23. Received 2009 May 18; in original form 2009 February 24

ABSTRACT

The description of the abundance and clustering of haloes for non-Gaussian initial conditions has recently received renewed interest, motivated by the forthcoming large galaxy and cluster surveys, which can potentially yield constraints of the order of unity on the non-Gaussianity parameter $f_{\rm NL}$. We present tests on *N*-body simulations of analytical formulae describing the halo abundance and clustering for non-Gaussian initial conditions. We calibrate the analytic non-Gaussian mass function of Matarrese, Verde & Jimenez and LoVerde et al. and the analytic description of clustering of haloes for non-Gaussian initial conditions on *N*-body simulations. We find an excellent agreement between the simulations and the analytic predictions if we make the corrections $\delta_c \longrightarrow \delta_c\sqrt{q}$ and $\delta_c \longrightarrow \delta_c q$, where $q \simeq 0.75$, in the density threshold for gravitational collapse and in the non-Gaussian fractional correction to the halo bias, respectively. We discuss the implications of this correction on present and forecasted primordial non-Gaussianity constraints. We confirm that the non-Gaussian halo bias offers a robust and highly competitive test of primordial non-Gaussianity.

Key words: methods: *N*-body simulations – methods: statistical – galaxies: clusters: general – galaxies: haloes – cosmology: theory – large-scale structure of Universe.

1 INTRODUCTION

Constraining primordial non-Gaussianity offers a powerful test of the generation mechanism of cosmological perturbations in the early Universe. While standard single-field models of slow-roll inflation lead to small departures from Gaussianity, non-standard scenarios allow for a larger level of non-Gaussianity (Bartolo et al. 2004 and references therein). The standard observables to constrain non-Gaussianity are the cosmic microwave background (CMB) and the large-scale structure (LSS) of the Universe. A powerful technique is based on the abundance (Koyama, Soda & Taruya 1999; Matarrese, Verde & Jimenez 2000; Robinson & Baker 2000; Robinson, Gawiser & Silk 2000; Verde et al. 2001; LoVerde et al. 2008) and clustering (Grinstein & Wise 1986; Matarrese, Lucchin & Bonometto 1986; Lucchin, Matarrese & Vittorio 1988) of rare events, such as dark matter density peaks, as they trace the tail of the underlying matter distribution. Theoretical predictions on various observational aspects of non-Gaussianity have been extensively tested against *N*-body simulations, leading to different and sometimes conflicting results (Dalal et al. 2007; Grossi et al. 2007; Kang, Norberg & Silk 2007; Pillepich, Porciani & Hahn 2008; Desjacques, Seljak & Iliev 2009).

Dalal et al. (2007) and Matarrese & Verde (2008) showed that primordial non-Gaussianity affects the clustering of dark matter haloes inducing a scale-dependent bias on large scales. Not only this effect has been already exploited to place stringent constraints on non-Gaussianity (Slosar et al. 2008; Afshordi & Tolley 2008), but also it is particularly promising for constraining non-Gaussianity from future surveys, which will provide a large sample of galaxy clusters over a volume comparable to the horizon size (e.g. DES, PanSTARRS, BOSS, LSST, ADEPT, EUCLID; Dalal et al. 2007; Afshordi & Tolley 2008; Carbone, Verde & Matarrese 2008; Seljak 2008). Bartolo, Matarrese & Riotto (2005) showed that even for

⋆E-mail: margot,dolag,iannuzzi@mpa-garching.mpg.de; verde,carbone@ieec.uab.es; branchin@fis.uniroma3.it; lauro.moscardini@unibo.it; sabino.matarrese@pd.infn.it

small primordial non-Gaussianities the evolution of perturbations on super-Hubble scales yields extra contributions. The amplitude of these contributions is comparable to the forecasted errors of some planned surveys, opening up the possibility of measuring them.

In light of this, it is important to use N-body experiments to test the validity of theoretical predictions for halo bias in non-Gaussian framework. Indeed, all proposed analytic biasing expressions have been derived in the extended Press–Schechter framework which assumes spherical collapse dynamics, sharp k-space filtering and Gaussian initial conditions. The validity of the extrapolation of the extended Press–Schechter approach to the non-Gaussian case can be tested independently by considering the halo mass function also. It is thus also important to test and calibrate on N-body simulations the predictions of the non-Gaussian halo mass function (Dalal et al. 2007; Grossi et al. 2007; Kang et al. 2007) and of the non-Gaussian halo bias simultaneously. This is what we set out to do here.

In this paper, we start by reviewing the analytic predictions for the Gaussian and non-Gaussian halo abundance and clustering (Section 2). In Section 3, we describe the numerical simulations with Gaussian and non-Gaussian initial conditions. In Section 4, we present the test for the non-Gaussian mass function. In Section 5 and 6, we test the analytic predictions of Gaussian and non-Gaussian large-scale bias against N-body simulations. In Section 7, we compare our results with the literature. Finally, we conclude in Section 8.

2 FORMULATION OF THE NON-GAUSSIAN HALO ABUNDANCE AND CLUSTERING

Deviations from Gaussian initial conditions are commonly parametrized in terms of the dimensionless $f_{\rm NL}$ parameter (Salopek & Bond 1990; Gangui et al. 1994; Verde et al. 2000; Komatsu & Spergel 2001):

$$\Phi = \phi + f_{\rm NL}(\phi^2 - \langle\phi^2\rangle)\,, \tag{1}$$

where Φ denotes the gravitational potential and ϕ is a Gaussian random field. As noted by, for example, LoVerde et al. (2008), Afshordi & Tolley (2008) and Pillepich et al. (2008), different authors use different conventions. Here, Φ denotes Bardeen's gauge-invariant potential which, on sub-Hubble scales, reduces to the usual Newtonian peculiar gravitational potential but with a negative sign. In addition, there are two conventions for normalizing equation (1): the LSS and the CMB one. In the LSS convention, Φ is linearly extrapolated at $z = 0$. In this paper, we use this convention. In the CMB convention, Φ is instead primordial (i.e. normalized deep in the matter-dominated era): thus, $f_{\rm NL} = [g(z=\infty)/g(0)]f_{\rm NL}^{\rm CMB} \sim 1.3 f_{\rm NL}^{\rm CMB}$, where $g(z)$ denotes the linear growth suppression factor in non-Einstein–de Sitter universes.

2.1 Formulation of the non-Gaussian mass function: extended Press–Schechter approach

In the Press–Schechter framework, one considers the density contrast field evaluated at some early time, far before any scale of interest has approached the non-linear regime, but extrapolated to the present day using linear perturbation theory. Then, one considers the height of the critical density threshold as a function of time. In that way, the collapse of a halo at redshift $z \neq 0$ corresponds to the $z = 0$ density fluctuation crossing a barrier of height $\delta_c(z) = \Delta_c D(z=0)/D(z)$, where $\Delta_c \sim \delta_c(z=0)$ (this is an equality only in an Einstein–de Sitter universe); we use $D(z=0) = 1$, $D(z) = g(z)/g(0)(1+z)^{-1}$. We should recall here that, even in linear theory, the normalized skewness of the density field, $S_3 \equiv \langle\delta^3\rangle/\langle\delta^2\rangle^2$, depends on redshift $\propto 1/D(z)$; however, in the Press–Schechter framework one should use the linear $S_3(z=0)$, in what follows $S_3 \equiv S_3(z=0)$. Also note that in general the skewness can be written as $S_3 \equiv f_{\rm NL} S_3^{(1)}$, where $S_3^{(1)}$ denotes the skewness in units of $f_{\rm NL}$, care must be exercised in the interpretation of $f_{\rm NL}$: if $S_3^{(1)}$ is that of the density field linearly extrapolated at $z = 0$, $f_{\rm NL}$ must be the LSS one and *not* the CMB one.

Generalization of the mass function to non-Gaussian initial conditions within the Press–Schechter formalism has been presented in Matarrese et al. (2000) and LoVerde et al. (2008). Both references start by computing an expression for the non-Gaussian probability density function of the smoothed dark matter density field, then obtain the level excursion probability. In the Press–Schechter approach, the mass derivative of the level excursion probability is the key ingredient to obtain the mass function expression and is the term that gets modified in the presence of primordial non-Gaussianity. In this derivation, several approximations are made. Both approaches assume that deviations from Gaussianity are small.

Matarrese et al. (2000) use first the saddle-point approximation to compute the level excursion probability and then truncate the resulting expression at the skewness. They obtain[1]

$$n(M,z) = 2\frac{3H_0^2\Omega_{\rm m,0}}{8\pi G M^2}\frac{1}{\sqrt{2\pi}\sigma_M}\exp\left(-\frac{\delta_*^2}{2\sigma_M^2}\right) \times \left|\frac{1}{2}\frac{\delta_c^2}{3\sqrt{1-S_{3,M}\delta_c/3}}\frac{{\rm d}S_{3,M}}{{\rm d}\ln M} + \frac{\delta_*}{\sigma_M}\frac{{\rm d}\sigma_M}{{\rm d}\ln M}\right|, \tag{2}$$

where σ_M denotes the rms value of the density field, the subscript M denotes that the density field has been smoothed on a scale $R(M)$ corresponding to $R(M) = [M3/(4\bar{\rho}_M)]^{1/3}$, and $\delta_* = \delta_c\sqrt{1-\delta_c S_{3,M}/3}$.

LoVerde et al. (2008) instead first approximate the probability density function using the Edgeworth expansion, then perform the integral of the level excursion probability exactly on the first few terms of the expansion. They obtain

$$n(M,z) = 2\frac{3H_0^2\Omega_{\rm m,0}}{8\pi G M^2}\frac{1}{\sqrt{2\pi}\sigma_M}\exp\left(-\frac{\delta_c^2}{2\sigma_M^2}\right) \times \left\{\frac{{\rm d}\ln\sigma_M}{{\rm d}M}\left[\frac{\delta_c}{\sigma_M} + \frac{S_{3,M}\sigma_M}{6}\left(\frac{\delta_c^4}{\sigma_M^4} - 2\frac{\delta_c^2}{\sigma_M^2} - 1\right)\right] + \frac{1}{6}\frac{{\rm d}S_{3,M}}{{\rm d}M}\sigma_M\left(\frac{\delta_c^2}{\sigma_M^2} - 1\right)\right\}. \tag{3}$$

Note that in the limit of small non-Gaussianity and rare events, the ratio of the non-Gaussian mass function to the Gaussian one for both expressions reduces to

$$\mathcal{R}_{\rm NG} \equiv \frac{n(M,z|f_{\rm NL})}{n(M,z|f_{\rm NL}=0)} \longrightarrow 1 + S_{3,M}\frac{\delta_c^3}{6\sigma_M^2}\,. \tag{4}$$

It is important to bear in mind that in equations (3) and (4) the redshift dependence is enclosed only in δ_c (and not in S_3). In the spirit of the 'CMB' convention instead, where the gravitational potential is normalized deep in the matter era, one should make sure that all the relevant quantities are correctly extrapolated linearly at $z = 0$, keeping in mind that the gravitational potential slowly evolves in a non-Einstein–de Sitter universe.

The major limitations in both derivations are the assumption of spherical collapse and the sharp k-space filtering. In addition,

[1] We correct here a typographical error in equation (68) of Matarrese et al. (2000), where ${\rm d}\ln\sigma_M$ should be ${\rm d}\sigma_M$.

the excursion set improvement on the interpretation of the original Press–Schechter swindle suggests that this derivation relies on the random-phase hypothesis (Sheth 1998), which is clearly not satisfied for non-Gaussian initial conditions even for sharp k-space filtering.

Verde et al. (2001) and LoVerde et al. (2008) addressed this issue by using the analytical approach to compute the fractional non-Gaussian *correction* to the Gaussian mass function $\mathcal{R}_{\rm NG}$, and used the Sheth & Tormen (1999) mass function to model the Gaussian mass function. This approach is potentially promising, but needs to be calibrated on numerical experiments.

In particular, one may argue that the same correction that in the Gaussian case modifies the collapse threshold and thus the form of the mass function from Press & Schechter (1974) to Sheth, Mo & Tormen (2001) and Sheth & Tormen (2002) may apply to the non-Gaussian correction. In the Gaussian case, this is usually referred to as the correction due to ellipsoidal collapse (Lee & Shandarin 1998). While this interpretation has recently been disputed (see e.g. Robertson et al. 2008), we will maintain the same nomenclature here. For rare events, high peaks ($\delta_c/\sigma_M \gg 1$) and small $f_{\rm NL}$, this is equivalent to lower δ_c by a factor $\sqrt{q}$ with $q = 0.75$.

In summary, we propose that the non-Gaussian mass function $n(M, z, f_{\rm NL})$ should be rewritten in terms of the Gaussian one $n_{\rm G}^{\rm sim}(M, z)$ – given by tested fits to simulations e.g. Sheth & Tormen (1999), Reed et al. (2003), Warren et al. (2006), Jenkins et al. (2001) – multiplied by a non-Gaussian correction factor:

$$n(M, z, f_{\rm NL}) = n_{\rm G}^{\rm sim}(M, z)\mathcal{R}_{\rm NG}(M, z, f_{\rm NL}), \tag{5}$$

where $R_{\rm NG}(M, z, f_{\rm NL})$ takes two different forms in the Matarrese et al. (2000) and LoVerde et al. (2008) approximations. For the Matarrese et al. (2000) case, [2]

$$R_{\rm NG}(M, z, f_{\rm NL}) = \exp\left[\delta_{\rm ec}^3 \frac{S_{3,M}}{6\sigma_M^2}\right] \times \left|\frac{1}{6}\frac{\delta_{\rm ec}}{\sqrt{1-\delta_{\rm ec}S_{3,M}/3}}\frac{{\rm d}S_{3,M}}{{\rm d}\ln\sigma_M} + \sqrt{1-\delta_{\rm ec}S_{3,M}/3}\right| \tag{6}$$

and for the LoVerde et al. (2008) case

$$R_{\rm NG}(M, z, f_{\rm NL}) = 1 + \frac{1}{6}\frac{\sigma_M^2}{\delta_{\rm ec}} \times \left[S_{3,M}\left(\frac{\delta_{\rm ec}^4}{\sigma_M^4} - 2\frac{\delta_{\rm ec}^2}{\sigma_M^2} - 1\right) + \frac{{\rm d}S_{3,M}}{{\rm d}\ln\sigma_M}\left(\frac{\delta_{\rm ec}^2}{\sigma_M^2} - 1\right)\right], \tag{7}$$

where $\delta_{\rm ec}$ denotes the critical density for ellipsoidal collapse, which for high peaks is $\delta_{\rm ec} \sim \delta_c\sqrt{q}$ with $q = 0.75$.

2.2 Formulation of the non-Gaussian large-scale halo bias

For the case of 'local' primordial non-Gaussianity equation (1), the analytical expression for the large-scale non-Gaussian bias has been derived in five different ways, obtaining always basically the same result. Dalal et al. (2007) considered the Laplacian of Φ in the vicinity of rare, high peaks, considering that the resulting $\nabla^2\Phi$ is proportional to the peaks overdensity; they also generalized to local non-Gaussianity the Kaiser (1984) argument of high-peaks bias in order to derive its non-Gaussian version. Matarrese & Verde (2008) derived the halo bias formula in general non-Gaussian cases specified by an expression for the bispectrum. Slosar et al. (2008) adopted the peak-background split approach (Cole & Kaiser 1989) for the local non-Gaussian case, showing that the resulting expression relies on the universality of the mass function. Afshordi & Tolley (2008) instead interpreted non-Gaussianity as a modification of the critical density for collapse, in the framework of ellipsoidal collapse. Finally, Taruya, Koyama & Matsubara (2008) – see also McDonald (2008) – used a perturbation theory approach to consider at the same time non-linear bias, second-order gravitational evolution and non-Gaussianity. It is encouraging that these different approaches yield a consistent result for the correction to the Gaussian Lagrangian halo bias $b_{\rm L}^{\rm G}$:

$$\frac{\Delta b}{b_{\rm L}^{\rm G}} = 2 f_{\rm NL}\delta_c(z)\alpha_M(k), \tag{8}$$

where $\alpha_M(k)$ encloses the scale and halo mass dependence – see Appendix and equation (13), and fig. 3 of Matarrese & Verde (2008). Also in this case the density field is the one extrapolated linearly at $z = 0$, and α_M does not depend on redshift.

Making the standard assumption that haloes move coherently with the underlying dark matter, the Lagrangian bias is related to the Eulerian one as $b = 1 + b_{\rm L}$.

The approximations used to derive this equation are Press–Schechter (Press & Schechter 1974) approach, linear bias, small non-Gaussianity, and in most cases spherical collapse and identification of peaks with haloes. It is therefore important to test the validity of equation (8) with simulations and see if any correction factor needed is indeed due to the account for non-spherical collapse/sharp k-filtering. Following the derivation of Matarrese & Verde (2008), we recognize that the correction to the two-point halo correlation function due to non-Gaussianity (their equation 6) is multiplied by ν^3/σ_M^3 with $\nu = \delta_c/\sigma_M$. In this factor, we recognize one Lagrangian Gaussian bias factor to the second power and an extra δ_c/σ_M^2, which denominator was absorbed in the form factor. Recall that, as discussed in Section 2.1, for 'ellipsoidal collapse' and rare events, the Lagrangian Gaussian bias is corrected as $\nu/\sigma_M \longrightarrow q\nu/\sigma_M$ (see equation 11 for high ν). However, the remaining factor is also a Gaussian bias and it should also be corrected by the q-factor.

We conclude that the 'non-spherical collapse' modifies equation (8) to be

$$\frac{\Delta b}{b_{\rm L}^{\rm G}} \simeq 2 f_{\rm NL}\delta_c(z)\alpha_M(k)q\,. \tag{9}$$

Note that Afshordi & Tolley (2008) arrived to a similar yet not identical expression when considering ellipsoidal collapse, i.e. they suggest that δ_c should be substituted by the critical density of Sheth et al. (2001), which in our limit would correspond to use $\sqrt{q}$ rather than q in equation (9).[3]

In Section 6, we will show that equation (9) correction fits well the simulations. Equation (9) is the first term of a Taylor series expansion and thus is valid only as long as expansion holds. For moderate values of $f_{\rm NL}$, large $\alpha(k)$ or very large $\delta_c(z)$, one should use more accurate expressions [4] (see Carbone et al. 2008 for more details).

3 *N*-BODY SIMULATIONS

The deviations from Gaussianity we are after become important on very large scales $k \lesssim 0.03\,h\,{\rm Mpc}^{-1}$ and for massive haloes.

[2] We correct here a typographical error in equation (3) of Grossi et al. (2007) where the exponential part was missing.

[3] With this substitution, however, the Gaussian bias would be corrected by a factor $\sqrt{q}$ rather than q as required by equation (11).

[4] For example, equation (9) may be written as $\sqrt{1 + 4 f_{\rm NL} q\delta_c(z)\alpha(k)} - 1$.

Therefore, one needs to perform N-body simulations on very large boxes, yet with enough resolution to identify massive virialized structures at different redshifts.

Suitable initial conditions have been set up following the method described in more detail in Grossi et al. (2008) (see also Grossi et al. 2007; Viel et al. 2009). In brief, a random realization of a Gaussian gravitational potential, $\Phi_{\rm L}$, normalized to be the one linearly extrapolated at $z = 0$, is generated in Fourier space, then it is inverse Fourier transformed back to real space and added to the non-Gaussian term, $\Phi_{\rm NL} = f_{\rm NL}(\Phi_{\rm L}^2 - \langle\Phi_{\rm L}^2\rangle)$. The resulting field $\Phi_{\rm L} + \Phi_{\rm NL}$ that is linear and at $z = 0$ is transformed back in Fourier space. We eventually modulate the power-law spectrum using the transfer function and compute the corresponding density field, which we then scale back to the initial condition redshift ($z = 60$). The corresponding gravitational potential is then used to displace particles according to the Zel'dovich approximation. This method allows one to simulate non-Gaussian models having power spectra which are all consistent with that of the Gaussian case and was already used by Viel et al. (2009).

In order to check the reliability of the initial condition generation, we have performed a specific test: using 256^3 particles in a box of size 1000 Mpc h^{-1}, primordial density fields (extrapolated linearly at $z = 0$) were generated and smoothed using spherical top-hat filters of different radii $r_s = 4, 6, 8, 12$ Mpc h^{-1}. The smoothed skewness was then extracted from the fields and compared to the analytical prediction for $f_{\rm NL} = 100, 200, 500, 1000$, as shown in Fig. 1.

The set of simulations used in this work assumes the 'concordance' Λ cold dark matter (ΛCDM) model. We fix the relevant parameters consistently with those derived from the analysis of the *Wilkinson Microwave Anisotropy Probe* (*WMAP*) 5-year data (Komatsu et al. 2009): $\Omega_{\rm m,0} = 0.26$ for the matter density parameter; $\Omega_{\Lambda 0} = 0.74$ for the Λ contribution to the density parameter; $h = 0.72$ for the Hubble parameter (in units of 100 km s^{-1} Mpc^{-1}). The initial power spectrum adopts the CDM transfer function suggested by Eisenstein & Hu (1999), has a spectral index $n = 0.96$ and is normalized in such a way that $\sigma_8 = 0.8$. In all experiments, performed using the GADGET-2 numerical code (Springel 2005), switching off the hydrodynamical part, we consider a box of $(1200\,{\rm Mpc}\,h^{-1})^3$ with 960^3 particles: the corresponding particle mass is then $m \approx 1.4 \times 10^{11}\,h^{-1}\,{\rm M}_\odot$. The gravitational force

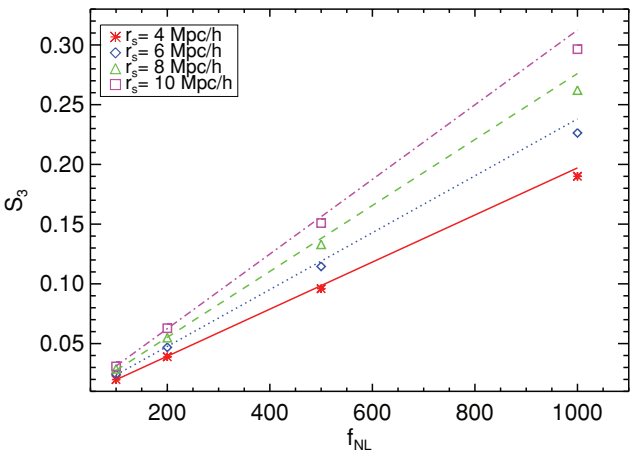

Figure 1. Skewness S_3 of the smoothed initial density field for $f_{\rm NL} = 100, 200, 500, 1000$. Symbols show the numerical results of the initial conditions code (averaged over five realizations) and are plotted against the analytical predictions for smoothing radii $r_s = 4, 6, 8, 10$ Mpc h^{-1} of a spherical top-hat filter.

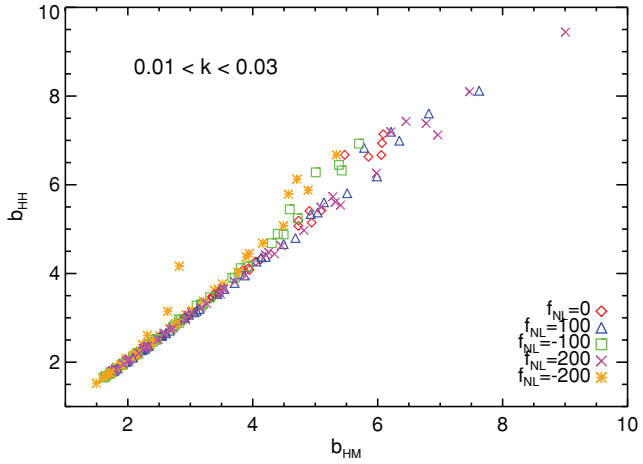

Figure 2. The bias of the halo power spectrum b_{hh} compared to the bias of the cross (halo matter) power spectrum b_{hm}. As expected, when the number density of haloes is high there is a good agreement between the two quantities. At low halo number densities, the two quantities are affected differently by shot noise, with b_{hm} being the least affected.

has a Plummer-equivalent softening length of $\epsilon_l = 25\,h^{-1}$ kpc. The runs produced 15 outputs from the initial redshift ($z = 60$) to the present time. The five simulations consider different amounts of primordial non-Gaussianity, parametrized by the $f_{\rm NL}$ parameter: $f_{\rm NL} = 0$ (i.e. the reference Gaussian case) and $f_{\rm NL} = \pm 100, \pm 200$. The catalogues of dark matter haloes are extracted from the simulations using the standard friends-of-friends algorithm adopting a linking length of 0.2 times the mean interparticle distance; only objects with at least 32 particles are considered.

We thus measure the halo bias in the simulations as

$$b_s(k, M, z) = b_{hm} \equiv \frac{P_{hm}(k, z, M)}{P_{mm}(k, z)}\,, \qquad (10)$$

where $P_{hm}(k, z, M)$ denotes the cross-power spectrum of dark matter with haloes of mass M at scale k, and for the simulation snapshot at redshift z. Similarly $P_{mm}(k, z)$ denotes the dark matter power spectrum. Here and hereafter, the subscript 's' denotes quantities measured from the simulation.

In principle, the quantity one is interested in would be the bias of the halo power spectrum $b_{hh} = \sqrt{P_{hh}/P_{mm}}$, but b_{hm} is a less noisy quantity [the shot noise of the finite number of haloes is greatly suppressed in the estimate of $P_{hm}(k)$]. The quantity b_{hm} is not guaranteed to be identical to b_{hh} if bias has a stochastic component that does not correlate with the matter density field. In Fig. 2, we show that this is not the case and that there is a good agreement on large scales between b_{hh} and b_{hm}, justifying using the less noisy b_{hm} as an estimator for b_{hh}.

3.1 Comparison with independent simulations

In Fig. 3, we show the mass function extracted from our Gaussian simulations at the following redshifts: $z = 0.0, 0.44, 1.02, 1.53, 2.26$ and 3.23. We also show three different theoretical predictions (also calibrated on N-body simulations): Sheth & Tormen (1999), Jenkins et al. (2001), Warren et al. (2006), solid, dotted and dashed lines, respectively. There is a good agreement even at high redshift.

The simulations used here are obtained with a different code for the initial conditions from Grossi et al. (2008), but we have checked that there is an agreement between the two sets of simulations. A visual comparison of the mass functions may be misleading; in fact,

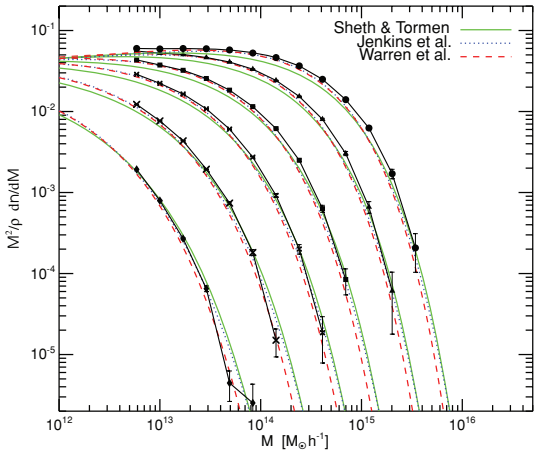

Figure 3. Multiplicity mass function for the Gaussian simulation computed using a friends-of-friends halo finder. Points denote the simulations results at different redshift: $z = 0, 0.44, 1.02, 1.53, 2.26$ and 3.23 (top to bottom). Solid (green) lines are the Sheth & Tormen (1999) formula, dashed (red) lines are the Warren et al. (2006) one and dotted (blue) are the Jenkins et al. (2001).

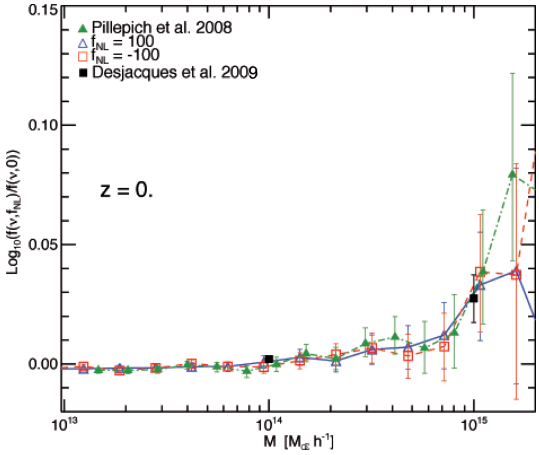

Figure 4. Comparison between the halo mass function recovered in our simulations with the work of Desjacques et al. (2009) and Pillepich et al. (2008) at $z = 0$. We show the ratio between our non-Gaussian and Gaussian simulation with $f_{\rm NL} = \pm 100$, few points we read out from fig. 1 of Desjacques et al. (2009) (black points) at the values of ν corresponding to 1×10^{13}, 1×10^{14} and $1 \times 10^{15}\,{\rm M}_{\odot}\,h^{-1}$ and the points from Pillepich et al. (2008). We plot the reciprocal of the results for $f_{\rm NL} = -100$.

the cosmologies used in the two simulations sets are different: here, we use a cosmology consistent with *WMAP* 5-year results while in Grossi et al. (2008) the cosmology in consistent with *WMAP* 1-year results. In addition, the box size and resolution differ: here, we have a volume of $(1200\,{\rm Mpc}\,h^{-1})^3$ and a mass resolution $m \sim 1.4 \times 10^{11}\,h^{-1}\,{\rm M}_{\odot}$ versus a volume of $(500\,{\rm Mpc}\,h^{-1})^3$ and a mass resolution $m \sim 2 \times 10^{10}\,h^{-1}\,{\rm M}_{\odot}$ of Grossi et al. (2008). A detailed comparison shows that despite the different volume, cosmological parameters, initial random seeds, the differences between the simulations are small (less than 10 per cent at $z = 0$) and negligible compared to the error bars . The larger simulation box enables us now to concentrate on the differential mass function, while Grossi et al. (2008) concentrated on the – less noisy – cumulative mass function. While we confirm here the results of a broad agreement between the theoretical predictions of the non-Gaussian mass functions and the simulations, the increased volume and halo number (by an order of magnitude) yield errors on the mass function smaller by a factor $\sim$3, making possible a robust 'detection' of the q-correction presented here. In addition, the larger simulation box enables us to study also the large-scale non-Gaussian halo bias.

More recently, several other groups presented N-body simulations, aiming at quantifying the effect of the non-Gaussian initial conditions on the halo mass function (Pillepich et al. 2008; Desjacques et al. 2009). All these results are obtained for similar cosmological parameters, so that we can compare estimates derived from all the simulations directly. By comparing the results for the individual simulations at $z = 1, z \sim 0.5$ and $z = 0$ in Figs 4 and 5, we demonstrate that these results are in agreement with the different groups, once the $f_{\rm NL}$ values are suitably converted to the same convention. Although all simulations use boxes of Giga parsec scales to explore the effect of non-Gaussian initial conditions at the high-mass end, the statistical errors at the scale of massive clusters are still large. Therefore, we also report the reciprocal of the results obtained for negative $f_{\rm NL}$ so that they appear in the positive part of the plot, to give an intuitive feeling of the noise within the individual simulations.

In Fig. 4, we show our simulation results for $f_{\rm NL} = 100$ (blue triangles) and for $f_{\rm NL} = -100$ (red squares) at $z = 0$ compared with data points from fig. 1 of Desjacques et al. (2009) (black points) at the values of ν corresponding to $1 \times 10^{13}, 1 \times 10^{14}$ and $1 \times 10^{15}\,{\rm M}_{\odot}\,h^{-1}$ (as given in their figure caption). Note that, as Desjacques et al. (2009) use $f_{\rm NL} = 100$ in the CMB convention for their simulations, we scaled the points down accordingly by a factor 1.3 to be comparable with our $f_{\rm NL} = 100$. We also show the results for Pillepich et al. (2008) (green points). Here, we again apply the rescaling as before, as their $f_{\rm NL}$ of 82 would correspond to a $f_{\rm NL}$ of $\sim$106 in the LSS notation.

In Fig. 5, the left-hand panel shows the results for Pillepich et al. (2008) (green points) at $z = 0.5$, and our points for the two closest available output times of our simulation ($z = 0.44$ and 0.61). The right-hand panel shows the comparison at $z = 1$ between our points (blue triangles and red squares) and points from Desjacques et al. (2009) (black squares).

From this comparison, we conclude that there is a remarkable agreement between the three independents simulations, highlighting the robustness of the simulations results. The differences visible at some of the highest mass bins are not significant, given the large error bars present.

4 MASS FUNCTION

We compare the halo mass function of the non-Gaussian simulations with the theoretical predictions of equations (5–7) that is including our *ansatz* for the non-spherical collapse correction: $\delta_c \longrightarrow \sqrt{q}\delta_c$. For clarity, we show here the non-Gaussian to Gaussian mass function ratio, i.e. the factor $R_{\rm NG}(M, z)$. The comparison between theory and simulations results is shown in Fig. 6 for a few redshift snapshots and for $f_{\rm NL} = \pm 100$, and in Fig. 7 for $f_{\rm NL} = \pm 200$ for the same redshifts. Dashed lines are the mass function of Matarrese et al. (2000) – equation (6) – and dot–dashed lines are that of LoVerde et al. (2008) – equation (7).

Contrary to Kang et al. (2007) and Dalal et al. (2007), we conclude that both Matarrese et al. (2000) and LoVerde et al. (2008) are good descriptions of the non-Gaussian correction to the mass function, once the correction for non-spherical collapse is included.

Figs 6 and 7 seem to indicate that LoVerde et al. (2008) may be a better fit for small masses while there is some tendency for

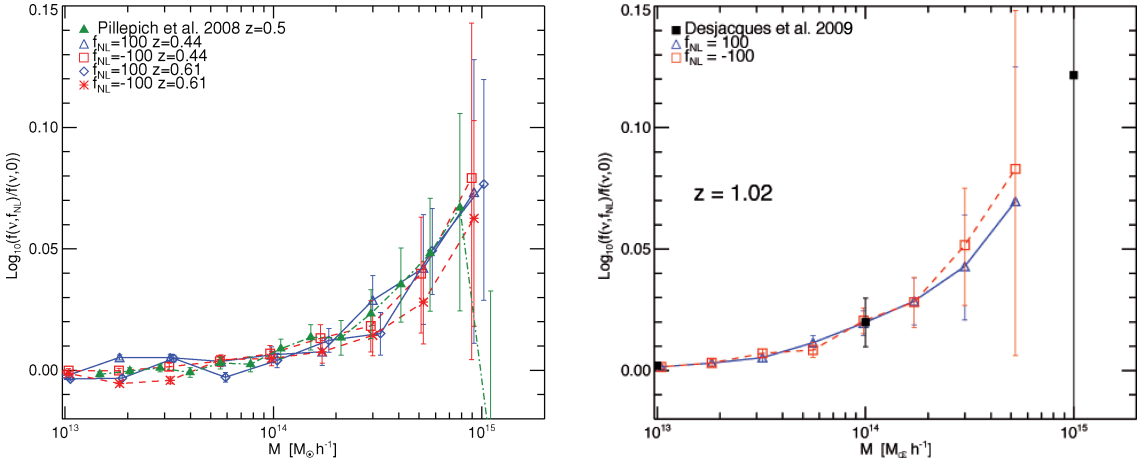

Figure 5. Comparison between the halo mass function recovered in our simulations with the work of Desjacques et al. (2009) and Pillepich et al. (2008). In both panels we show the ratio between the non-Gaussian and Gaussian simulation points. In the left-hand panel, we show the data of Pillepich et al. (2008) at $z = 0.5$ and compare them with our simulation results for the two closest available redshifts: $z = 0.44$ and 0.61 and with Desjacques et al. (2009). In the right-hand panel, we show the points at redshift 1 for our simulations with $f_{\rm NL} = \pm 100$ and three points we read out from fig. 1 of Desjacques et al. (2009) (black points) at the values of ν corresponding to 1×10^{13}, 1×10^{14} and 1×10^{15} $\mathrm{M}_{\odot}\, h^{-1}$. We plot the reciprocal of the results for $f_{\rm NL} = -100$. All points are rescaled to $|f_{\rm NL} = 100|$ in our notation. The three independent simulations are in good agreement.

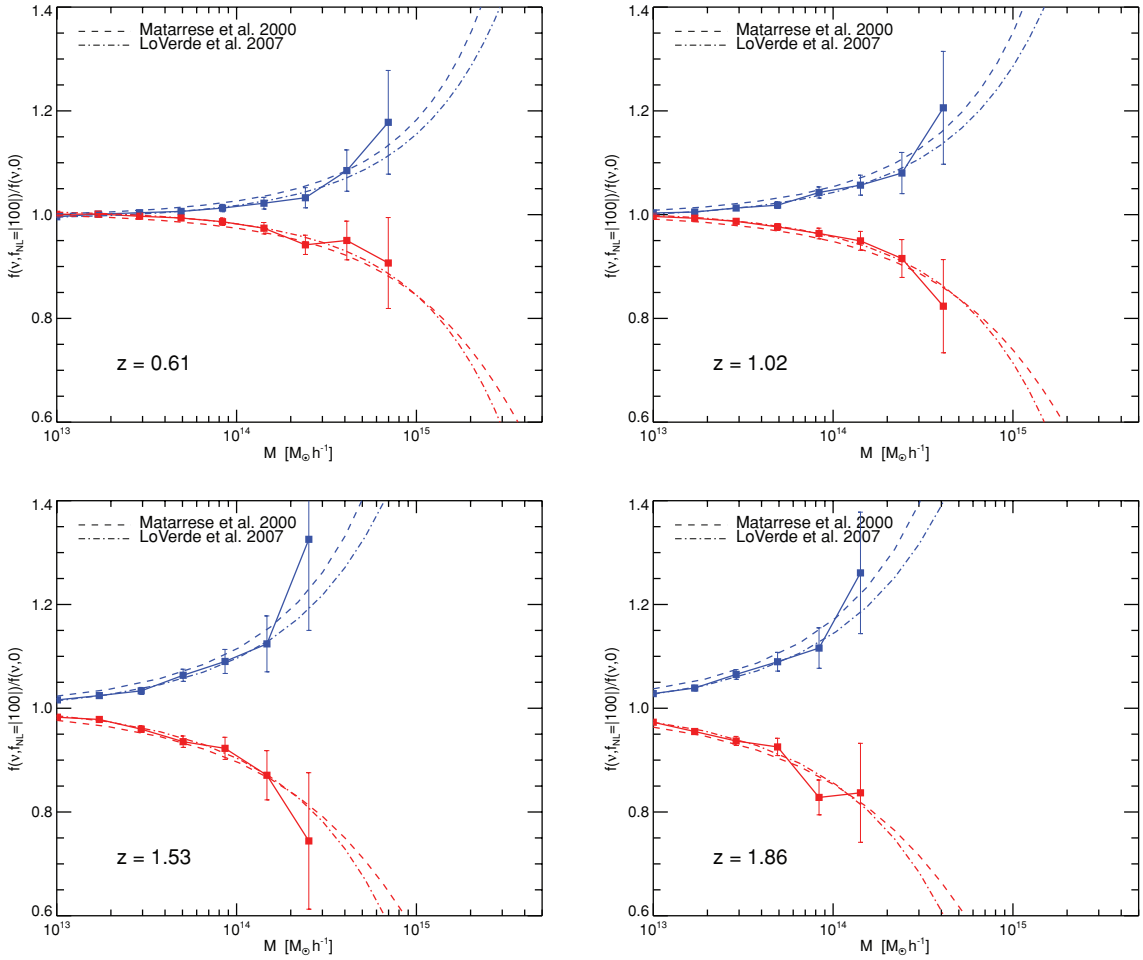

Figure 6. Ratio of the non-Gaussian ($f_{\rm NL} = \pm 100$) to Gaussian mass function for different redshift snapshots: top-left panel $z = 0.61$; top-right panel $z = 1.02$; bottom-left panel $z = 1.53$; bottom-right panel $z = 1.86$. The dashed line is the mass function of Matarrese et al. (2000) and the dot–dashed lines are that of LoVerde et al. (2008), both including the q-correction.

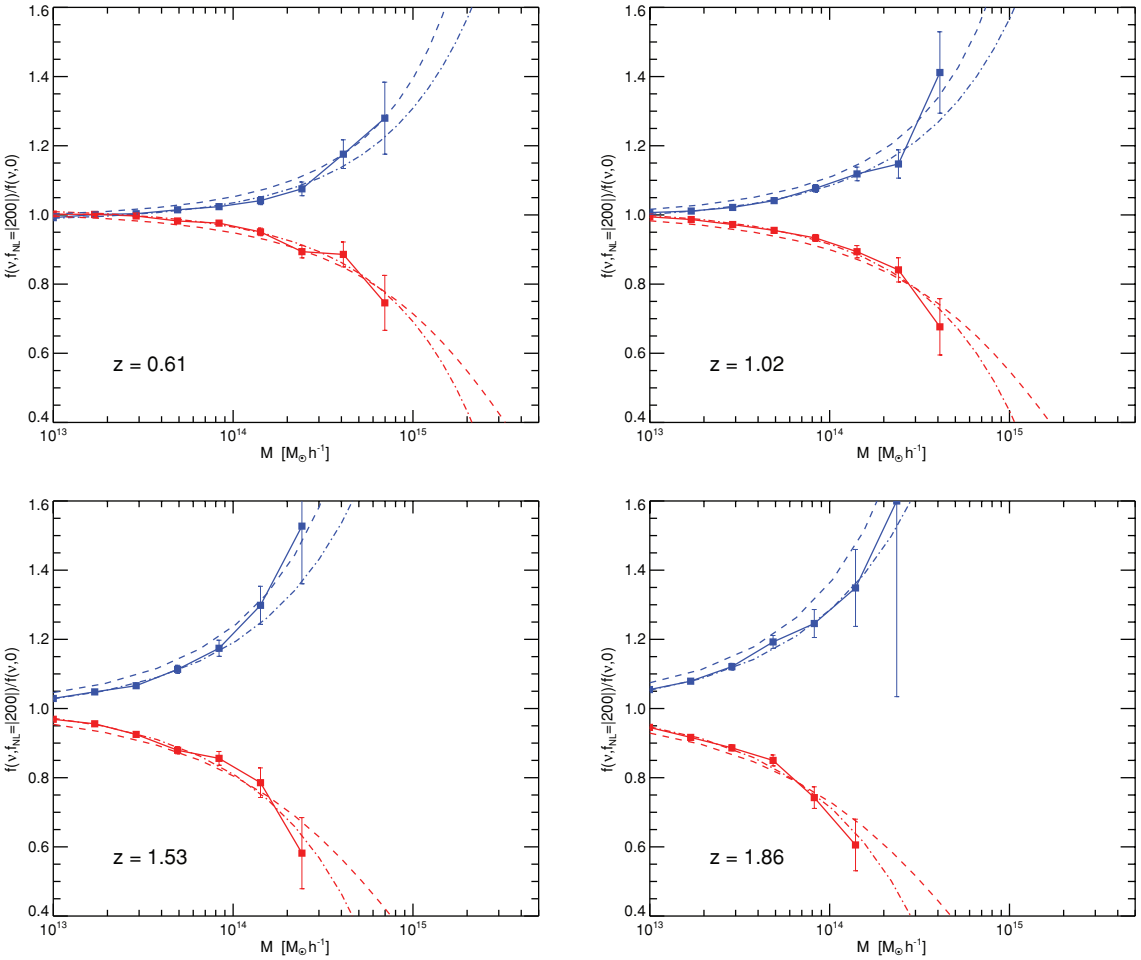

Figure 7. Ratio of the non-Gaussian ($f_{\rm NL} = \pm 200$) to Gaussian mass function for different redshift snapshots: top-left panel $z = 0.61$; top-right panel $z = 1.02$; bottom-left panel $z = 1.53$; bottom-right panel $z = 1.86$. The dashed line is the mass function of Matarrese et al. (2000) and the dot–dashed lines are that of LoVerde et al. (2008), both including our q-correction.

Matarrese et al. (2000) to provide a better fit at high masses. This is not surprising: the Edgeworth expansion works well away from the extreme tails of the distribution (i.e. for moderate δ_c/σ_M), while the saddle-point approximation used in Matarrese et al. (2000) is expected to work better at the very tails of the distribution (very high δ_c/σ_M). We expect that the mass function of Matarrese et al. (2000) will be a better fit at very high masses or larger $f_{\rm NL}$. This will be further explored in future work.

5 GAUSSIAN HALO BIAS, AND THE EFFECT OF MERGERS

The large-scale, linear halo Eulerian bias for the Gaussian case is (Mo & White 1996; Mo, Jing & White 1997; Scoccimarro et al. 2001)

$$b^{\rm G} = 1 + \frac{1}{D(z_{\rm o})}\left[\frac{q\delta_c(z_{\rm f})}{\sigma_M^2} - \frac{1}{\delta_c(z_{\rm f})}\right] + \frac{2p}{\delta_c(z_{\rm f})D(z_{\rm o})}\left\{1 + \left[\frac{q\delta_c^2(z_{\rm f})}{\sigma_M^2}\right]^p\right\}^{-1}, \quad (11)$$

where $q = 0.75$ and $p = 0.3$ account for non-spherical collapse and are a fit to numerical simulations. Here, σ_M denotes the rms value of the dark matter fluctuation field smoothed on a scale R corresponding to the Lagrangian radius of the haloes of mass M; $z_{\rm f}$ denotes the halo formation redshift and $z_{\rm o}$ denotes the halo observation redshift. As we are interested in massive haloes, we expect that $z_{\rm f} \simeq z_{\rm o}$. As the non-Gaussian halo bias correction is proportional to $b^{\rm G} - 1$, the dependence of $b^{\rm G}$ on whether the selected haloes underwent a recent merger (i.e. $z_{\rm f} \sim z_{\rm o}$) or are old haloes (i.e. $z_{\rm f} \gg z_{\rm o}$) affects the amplitude of the non-Gaussian correction (Carbone et al. 2008; Slosar et al. 2008). Before we trust our simulation to accurately describe the non-Gaussian halo bias, we check whether we recover the Gaussian one and whether the linear halo bias approximation is a good description for the scales, redshifts and mass ranges we are interested in. Gao, Springel & White (2005) show that analytical predictions for the Gaussian halo bias are in reasonable agreement with simulations and that the bias for low-mass haloes shows strong dependence on formation time but high-mass haloes (the ones we are interested in) do not. The halo bias for the Gaussian simulation and the comparison with the theory prediction are shown in Fig. 8. Except for the Gaussian halo bias $b_0^{\rm G} \equiv 1 + \delta_c(z_{\rm o})/[\sigma_M^2 D(z_{\rm o})]$ defined in Efstathiou et al. (1988) and Kaiser (1984) indicated by the dotted (blue) line, the simulated data agree with the theoretical expectations at different redshifts. In particular, in Fig. 8, the black solid line represents the total Gaussian bias of equation (11), the dashed (red) line represents the contribution from the first line of equation (11) and, finally, the dot–dashed (green) line is

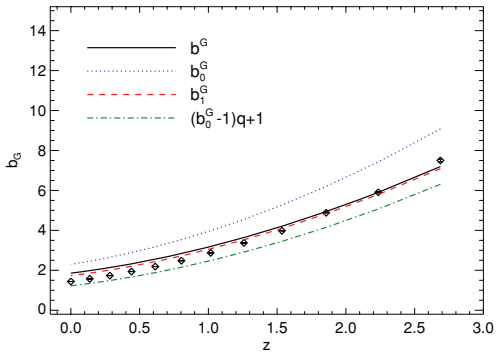

Figure 8. Black solid line: the large-scale Gaussian halo Eulerian bias $b^{\rm G}$ of equation (11). Blue dotted line: the Gaussian halo bias $b_0^{\rm G} \equiv 1 + \delta_c(z_{\rm o})/[\sigma_M^2 D(z_{\rm o})]$ as defined in Efstathiou et al. (1988) and Kaiser (1984). Green dot–dashed line: $1 + q(b_0^{\rm G} - 1)$. Red dashed line: the contribution $b_1^{\rm G} \equiv 1 + [q\delta_c(z_{\rm f})/\sigma_M^2 - 1/\delta_c(z_{\rm f})]/D(z_{\rm o})$ to the total bias of equation (11).

$1 + q(b_0^{\rm G} - 1)$. The small difference when using $z_{\rm f} \sim z_{\rm o}$ implies that, for the Gaussian halo bias of very massive haloes ($M \gtrsim 10^{13}\,{\rm M}_\odot$), it is reliable to assume that the correction from the 'non-spherical collapse' can be encapsulated in the factor q in front of $\delta_c(z_{\rm o})/[\sigma_M^2 D(z_{\rm o})]$.

6 NON-GAUSSIAN HALO BIAS

The effect of non-Gaussian halo bias on the halo matter cross-power spectrum is shown in Fig. 9, where we considered haloes of mass above $10^{13}\,{\rm M}_\odot$ in the simulation snapshot at $z = 1.02$. The bottom panel of Fig. 9 shows the non-Gaussian bias relative to the Gaussian one. Note that error bars in the upper panel include cosmic variance error. The relative bias in the lower panel is obtained from the ratio of the non-Gaussian to Gaussian power spectra, in this quantity the cosmic variance is greatly reduced as the Gaussian components of the initial conditions are in common. Here and in the following Figs 10 and 14, the error bars shown are the error on the average of the band-power quantity shown in the y-axis.

While Fig. 9 only qualitatively illustrates the effect, a more quantitative comparison between the simulation results and the theory

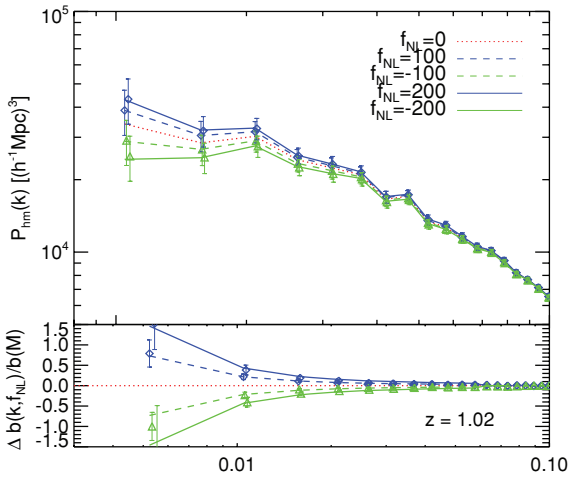

Figure 9. Effect of the non-Gaussian halo bias on the power spectrum. In the top panel, we show the halo matter cross-power spectrum for masses above $10^{13}\,{\rm M}_\odot$ at $z = 1.02$. The bottom panel shows the ratio of the non-Gaussian to Gaussian bias.

is presented in Fig. 10, where we show that the quantity $\Delta b/b$ of equation (8) obtained from the simulations outputs (points with error bars) and the corresponding theory lines as a function of k, for selected redshift snapshots of the simulations. We have considered halo masses above $10^{13}\,{\rm M}_\odot$. It is clearly visible from Fig. 10 that the non-Gaussian halo bias effect becomes increasingly more pronounced at high redshift and larger scales for a fixed halo mass range.

For a more detailed comparison between theory and simulations and quantitative evaluation of the performance of the 'q-correction we introduced, we proceed as follows. We note that in equation (8) the redshift and scale dependence of the non-Gaussian correction can be factorized as a term that depends only on redshift and one that depends only on k and M. The M-dependence is expected to be very weak at large scales ($k < 0.03\,h^{-1}\,{\rm Mpc}^{-1}$). Here, we will test the mass, scale and redshift dependence of the non-Gaussian halo bias and calibrate its normalization on the simulations.

In Fig. 11, we show the dependence on halo mass of $\Delta b/b_{\rm L}$. We define the quantity

$$\mathcal{R}(M) = \left(\frac{\Delta b}{b_{\rm L}}\right)_s \left(\frac{\Delta b}{b_{\rm L}}\right)^{-1}_{\rm theory}, \qquad (12)$$

where $(\Delta b/b_{\rm L})_{\rm theory}$ is given by equation (8). To study the mass dependence, we evaluate the theory at fixed mass $\widehat{M} = 10^{14}\,{\rm M}_\odot$. We compute the bias from the simulations taking haloes in six different mass bins. Fig. 11 includes only scales $k < 0.03\,h\,{\rm Mpc}^{-1}$, different lines correspond to different redshift snapshots between $z = 0$ and 1.5. As expected, there is no notable dependence on halo mass.

Having confirmed the expected weak dependence on halo mass for masses $M > 10^{13}\,{\rm M}_\odot/h$ and on scales $k < 0.03\,h\,{\rm Mpc}^{-1}$, we can study the redshift and scale dependence of $\Delta b/b_{\rm L}$, considering haloes of different masses above $10^{13}\,{\rm M}_\odot\,h^{-1}$.

The redshift dependence of $\Delta b/b_{\rm L}$, $(\Delta b/b_{\rm L}^{\rm G})_s[2f_{\rm NL}\alpha_M(k)q]^{-1}$ is shown in Fig. 12 where $M > 10^{13}\,{\rm M}_\odot/h$ and scales $k < 0.026\,h\,{\rm Mpc}^{-1}$ were used. In applying the correction $\delta_c/\sigma_M^2 \longrightarrow q\delta_c/\sigma_M^2$ to $\Delta b/(b_{\rm G} - 1)$, we have actually corrected $b_0^{\rm G}$, i.e. we have employed the same approximation used for the green dot–dashed line of Fig. 8, giving equation (9). Equation (9) in fact is only the consequence of our correction to the Gaussian halo bias. Note that the approximation $z_{\rm f} \sim z_0$ we employed here is expected to hold for rare – massive – haloes, and Fig. 8 shows that this is a good approximation. A detailed study of the dependence of the non-Gaussian halo bias correction on the formation redshift of the haloes will be presented elsewhere.

There seems to be an indication that the q-correction factor for the large-scale bias correction may slightly depend on the value of $f_{\rm NL}$: in particular, the figure shows that it could be slightly smaller than q for $f_{\rm NL}$ large and negative and smaller for $f_{\rm NL}$ large and positive. This is not unexpected for two reasons: first, for large non-Gaussianity the Taylor expansion done to obtain equation (8) (see derivation of equation 13 of Matarrese & Verde 2008) looses accuracy at high redshift; secondly, the presence of non-Gaussianity may alter the dynamics of non-spherical collapse [e.g. through tidal forces – see e.g. Desjacques (2009) – or by significantly changing the redshift for collapse with respect to the Gaussian case]. At this stage, however, this trend is not highly significant and further study will be left to future work.

We show the scale dependence of equation (9), $(\Delta b/b_{\rm L}^{\rm G})_s[2f_{\rm NL}\delta_c(z)q]^{-1}$, in Fig. 13. The thin lines correspond to different redshifts and the thick black line to their average. The dotted line is the theory prediction with $q = 0.75$. Note

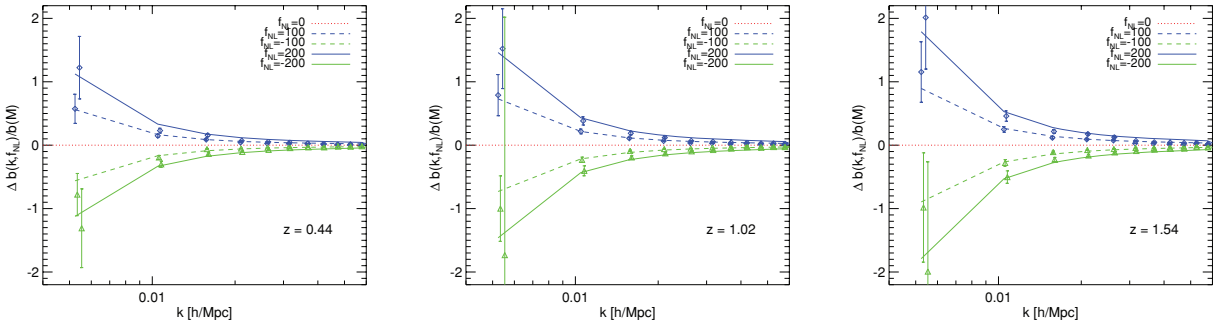

Figure 10. The quantity of equation (8), $\Delta b/b$ as function of k, for simulation snapshots at $z = 0.44$, 1.02 and 1.54. Simulation outputs and theory lines are shown for $f_{\rm NL} = \pm 100$ and ± 200.

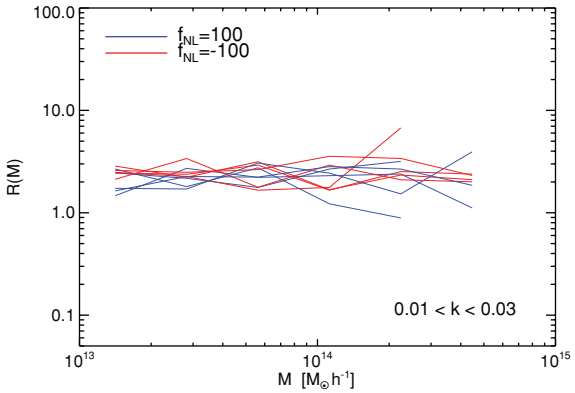

Figure 11. Weak mass dependence of $\Delta b/b$ at scales $k < 0.03\,h^{-1}\,{\rm Mpc}^{-1}$. Different lines correspond to different redshift snapshots between $z = 0$ and 1.5. The overall normalization is arbitrary.

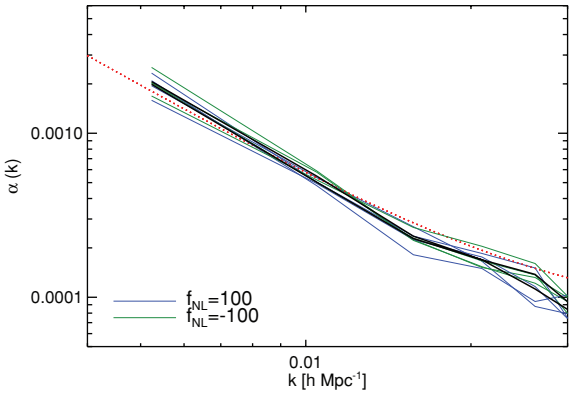

Figure 13. Scale dependence of equation (9). The thin lines correspond to different redshifts for haloes with mass above $10^{13}\,{\rm M}_\odot/h$ and the thick black line is their average. The dotted line is the theory prediction with $q = 0.75$. At $k > 0.03\,h\,{\rm Mpc}^{-1}$, the effect of non-Gaussianity is very small, and the measurement becomes extremely noisy.

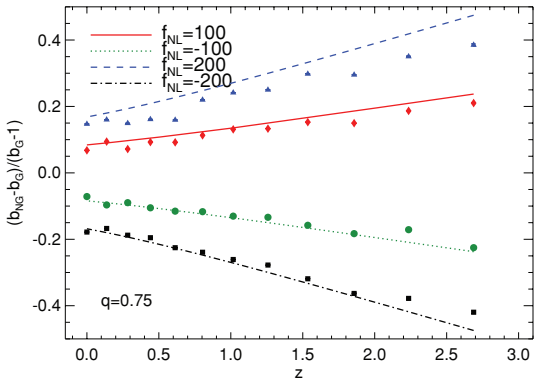

Figure 12. The redshift dependence of the non-Gaussian correction to the halo bias: points are the values measured from the simulations and lines are the theoretical predictions, equation (9). Only $k < 0.026\,h\,{\rm Mpc}^{-1}$ were used.

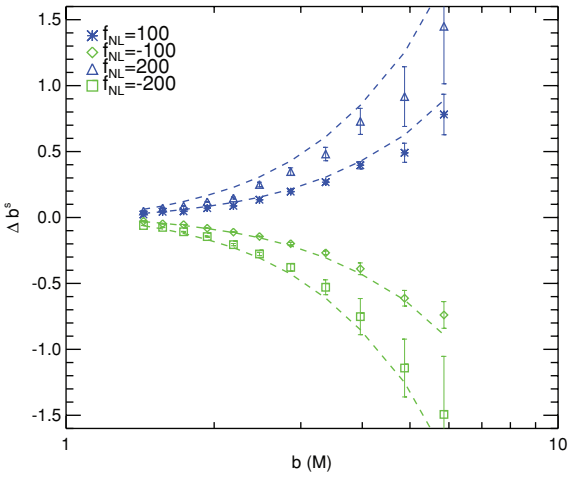

Figure 14. Non-Gaussian halo bias correction as function of the Gaussian halo bias.

that there is an excellent agreement on the scales of interest, e.g. $k < 0.03\,h\,{\rm Mpc}^{-1}$. On smaller scales, the effect of non-Gaussianity is very small and the measurement become extremely noisy. These results are in qualitative agreement with the findings of Pillepich et al. (2008).

Finally, in Fig. 14 we show the non-Gaussian halo bias correction Δb from the simulations as function of the Gaussian halo bias. We only consider scales $k < 0.03$.

We conclude that equation (9), with $q \sim 0.75$, provides a good fit to non-Gaussian simulations.

7 COMPARISON WITH PREVIOUS WORK

After the discussion of Section 2, it should be clear that if $f_{\rm NL}^{\rm CMB}$ were used in the theoretical predictions or S_3 were *not* linearly extrapolated to $z = 0$, then any constraints on non-Gaussianity so obtained would have to be rescaled by a factor $\sim$1.3. This seems to be the case of some work in the literature. On the other hand, the q-correction factor effectively introduces a rescaling of a factor

$\sim 0.75^{3/2} = 0.65$ for the mass function case and 0.75 for the bias case. It is a coincidence that, for the halo bias, $1.3 \times 0.75 \sim 1$, thus the $f_{\rm NL}$ normalization mistake cancels out with the spherical collapse approximation error. This fortuitous cancellation does not happen to the same level in the mass function $0.75^{3/2} \times 1.3 \sim 0.8$, explaining perhaps some of the claimed discrepancy of the simulations with the analytic mass function predictions and the claimed agreement with the halo bias predictions. Another possible source of inaccuracy would be an inconsistent treatment of the redshift evolution of δ_c and S_3 (see discussion in Section 2).

The simulations used here are obtained with a different code for the initial conditions from Grossi et al. (2008), but we have checked that there is an agreement between the two sets of simulations. A visual comparison of the mass functions may be misleading; in fact, the cosmologies used in the two simulations sets are different: here, we use a cosmology consistent with *WMAP* 5-year results while in Grossi et al. (2008) the cosmology in consistent with *WMAP* 1-year results. In addition, the box size and resolution differ: here, we have a volume of $(1200\,{\rm Mpc}\,h^{-1})^3$ and a mass resolution $m \sim 1.4 \times 10^{11}\,h^{-1}\,{\rm M}_\odot$ versus a volume of $(500\,{\rm Mpc}/h)^3$ and a mass resolution $m \sim 2 \times 10^{10}\,h^{-1}\,{\rm M}_\odot$ of Grossi et al. (2008). A detailed comparison shows that despite the different volume, cosmological parameters, initial random seeds, the differences between the simulations are small (less than 10 per cent at $z = 0$) and negligible compared to the error bars. The larger simulation box enables us now to concentrate in detail on the differential mass function, while Grossi et al. (2008) concentrated on the cumulative mass function. While we confirm here the results of a broad agreement between the theoretical predictions of the non-Gaussian mass functions and the simulations, the increased volume and halo number (by an order of magnitude) yield errors on the mass function smaller by a factor >3, making possible a robust 'detection' of the q-correction presented here. In addition, the larger simulation box enables us to study also the large-scale non-Gaussian halo bias.

In Fig. 15, we compare our theoretical predictions with the results presented in Pillepich et al. (2008) and Desjacques et al. (2009). The left-hand panel shows our simulation results at $z = 0$ for $f_{\rm NL} = \pm 100$ and our theoretical predictions. Additionally, we show the fit presented by Pillepich et al. (2008), equations (8) and (9), evaluated for the suitable values of $f_{\rm NL}$ accounting for the different notations for $f_{\rm NL}$. We also adopt our cosmological parameters when converting σ_M to M. The right-hand panel shows the simulation results presented in Pillepich et al. (2008) at $z = 0$ and their fitting formula at $z = 0$ and 1. We over plot our theoretical models evaluated for their cosmological parameters and for the corresponding values of $f_{\rm NL}$. Moreover, we add the data points from Desjacques et al. (2009) for $z = 0$ and 1, suitably rescaled by the differences of the $f_{\rm NL}$ value used. The mass function fits of Fig. 12 differ for large masses, in the regime where simulations errors become large; the fits are, however, consistent given the individual points error bars.

Our theoretical formulae for the non-Gaussian mass function (equations 5–7) and for the non-Gaussian halo bias (equation 9) are physically motivated expressions that have been tested on N-body simulations. They have the advantage over fitting formulae that they can be more robustly interpolated and extrapolated to cosmologies and parameters that have not been directly simulated, and they are more robust over parameters ranges where the simulations have low signal-to-noise ratio. Compared to simple fitting formulae, equations (6), (7) and (9) have the disadvantage that they require the calculation of some numerical integrals. To overcome this, we supply tabulated values for $S^{(1)}_{3,M}, \sigma_M$ and α_M for a *WMAP5* cosmology in the range of interest at www.ice.csic.es/personal/verde/nongaussian.html.

The q-correction we find here has implications for previously reported and forecasted constraints on non-Gaussianity. In Table 1, we report present and forecasted constraints on $f_{\rm NL}$ from the literature rescaled to $f^{\rm CMB}_{\rm NL}$ and corrected for our factor q.

This confirms that constraints on $f_{\rm NL}$ for non-Gaussianity of the local type, achievable using the non-Gaussian halo bias, are competitive with CMB constraints ($f_{\rm NL} \sim 5$ for Planck and $f_{\rm NL} \sim 3$ for a CMB Pol-type mission; Babich & Zaldarriaga 2004; Yadav, Komatsu & Wandelt 2007).

8 CONCLUSIONS

We have considered $(1.2\,{\rm Gpc}\,h^{-1})^3$ size and 960^3 particles N-body simulations with non-Gaussian initial conditions of the local type, with non-Gaussianity parameter $f_{\rm NL} = \pm 100$, $f_{\rm NL} = \pm 200$ and a reference Gaussian simulation ($f_{\rm NL} = 0$). The clustering properties and the abundance of the simulation's haloes were then compared

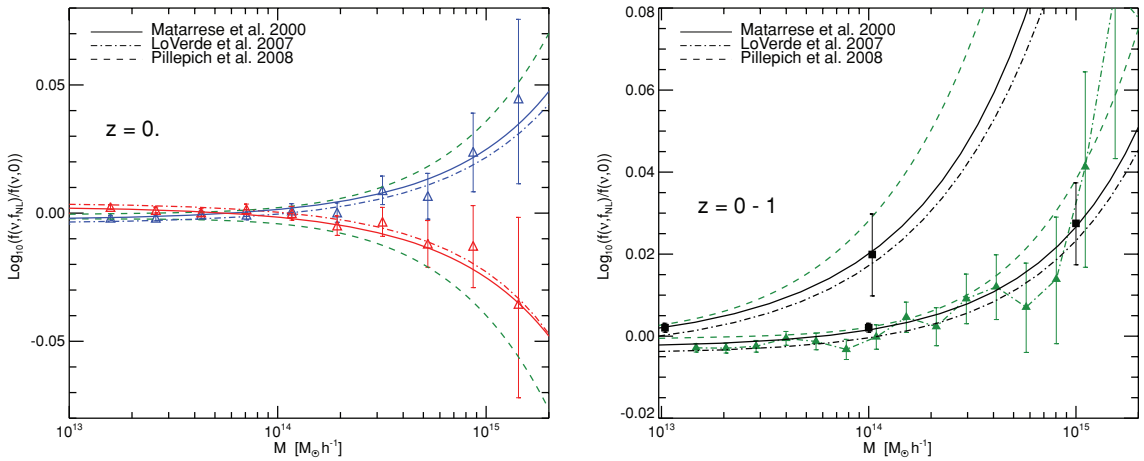

Figure 15. Left-hand panel: comparison between simulations points and fits from this work and the polynomial fit of Pillepich et al. (2008). Right-hand panel: our correction to the Matarrese et al. (2000) and LoVerde et al. (2008) non-Gaussian mass function fits, the polynomial fit of Pillepich et al. (2008) and points from Desjacques et al. (2009) (black squares) and Pillepich et al. (2008) (green triangles). See the text for more details.

Table 1. Current and forecasted constraints on $f_{\rm NL}^{\rm CMB}$.

Data/method	Measurements $f_{\rm NL}$, 1σ–2σ errors	Reference
Photo-LRG–bias	$84^{+54+101}_{-85-331}$	Slosar et al. (2008)
Spectro-LRG–bias	$93^{+74+139}_{-83-191}$	Slosar et al. (2008)
QSO–bias	11^{+26+47}_{-37-77}	Slosar et al. (2008)
Combined	37^{+23+42}_{-26-57}	Slosar et al. (2008)
NVSS–ISW	$140^{+647+755}_{-337-1157}$	Slosar et al. (2008)
NVSS–ISW	272 ± 127 (2σ)	Afshordi & Tolley (2008)
Data/method	Forecasts $\Delta f_{\rm NL}(1-\sigma)$	Reference
BOSS–bias	18	Carbone et al. (2008)
ADEPT/Euclid–bias	1.5	Carbone et al. (2008)
PANNStarrs–bias	3.5	Carbone et al. (2008)
LSST–bias	0.7	Carbone et al. (2008)
LSST–ISW	10	Afshordi & Tolley (2008)

with independent simulations and theoretical predictions. We find a good agreement between different simulations, indicating that the initial conditions setup is under control. We find that the Press–Schechter-based description of the non-Gaussian correction to the Gaussian mass function of Matarrese et al. (2000) and LoVerde et al. (2008) is a good fit to the simulations, provided that

(i) the Press–Schechter-based description is used to compute the ratio between Gaussian and non-Gaussian mass function and
(ii) the critical density δ_c is corrected to account for non-spherical collapse dynamics.

This is summarized in our equation (5) and in equations (6) and (7) for the non-Gaussian mass functions of Matarrese et al. (2000) and LoVerde et al. (2008), respectively. For large thresholds this correction is equivalent to a rescaling of the spherical collapse threshold: $\delta_c\sqrt{q}$ where $q = 0.75$. The q-correction is thus equivalent to a reduction of $f_{\rm NL}$ by a factor $\sim$1.5 because in the mass function, to leading order $f_{\rm NL}$ multiplies δ_c^3.

We find that the non-Gaussian halo bias prescription of Dalal et al. (2007), Matarrese & Verde (2008), Slosar et al. (2008) and Afshordi & Tolley (2008) provides a good description of the scaling of the large-scale halo clustering of the simulations. In particular, we have tested separately the predicted redshift, scale and $f_{\rm NL}$ dependence. The overall amplitude of the effect, however, should be corrected by a factor $\sim q$ which can also be understood in the context of ellipsoidal collapse or as a modification to the excursion set ansatz and the sharp k-space filtering (see equation 9). There is an indication that this correction may be slightly dependent on $f_{\rm NL}$. This is not unexpected, but the signal-to-noise ratio of the effect is too small in the current simulations to draw robust conclusions. We also find that on large ($k < 0.03\,h\,{\rm Mpc}^{-1}$) scales, as expected, the fractional correction to the non-Gaussian halo bias is independent of mass. On smaller scales a dependence on mass is expected, but the simulations do not have sufficient signal-to-noise ratio to verify it. The q-correction to the non-Gaussian halo bias modifies current and forecasted constraints reported in the literature as indicated in our Table 1.

The formulae we presented here for the non-Gaussian mass function (equations 5–7) and non-Gaussian halo bias (equation 9) are physically motivated expressions which provide good fits to a suite of N-body simulations. As such, they can be more robustly interpolated and extrapolated than simple fitting functions (in www.ice.csic.es/personal/verde/nongaussian.html, we provide useful quantities for ease of use of these equations.). We confirm that the non-Gaussian halo bias offers a robust and highly competitive test of primordial non-Gaussianity of the local type.

After the present work was submitted, closely related works by Maggiore and Riotto were posted to the on-line repository (arXiv:0903.1251 and arXiv:0903.1250). In their work, a physical interpretation of the q-correction of the non-Gaussian mass function presented here is offered. In particular, they show that the q-coefficient can be understood in terms of the diffusing barrier model, which is responsible for modifications both to the Gaussian and non-Gaussian mass function. The fact that the same effect should appear in both the Gaussian and non-Gaussian mass function is discussed here also in Section 2.1. It may be worth mentioning that Borgani & Bonometto (1990) indicated that modifying the shape of the barrier (i.e. assuming that the δ_c threshold is not strictly a step function) would lead to a modification of the mass function in a similar direction.

ACKNOWLEDGMENTS

Computations have been performed on the IBM-SP5 at Consorzio Interuniversitario del Nord-Est per il Calcolo Automatico (CINECA), Bologna, with CPU time assigned under an INAF-CINECA grant, and on the IBM-SP4 machine at the 'Rechenzentrum der Max-Planck-Gesellschaft' at the Max-Planck-Institut fuer Plasmaphysik with CPU time assigned to the 'Max-Planck-Institut für Astrophysik' and at the 'Leibniz-Rechenzentrum' with CPU time assinged to the Project 'h0073'. The authors thank A. Pillepich and C. Porciani for discussions and for making available the simulations outputs for comparison. We also thank N. Dalal, U. Seljak, A. Riotto and M. Maggiore for discussions. LV is supported by FP7-PEOPLE-2007-4-3-IRG n. 202182 and CSIC I3 grant no. 200750I034. CC is supported through a Beatriu de Pinos grant. This research was supported by the DFG cluster of excellence Origin and Structure of the Universe. SM and LM acknowledge partial support by ASI contract I/016/07/0 'COFIS', ASI-INAF I/023/05/0, ASI-INAF I/088/06/0 and ASI contract Planck LFI Activity of Phase E2. LV thanks the Santa Fe cosmology workshop 2008, LV and CC thank the Galileo Galilei Institute for theoretical physics in Florence, where part of this work was carried out, and INFN for partial support. LV thanks B. Wandelt for discussions.

REFERENCES

Afshordi N., Tolley A. J., 2008, Phys. Rev. D, 78, 123507
Babich D., Zaldarriaga M., 2004, Phys. Rev. D, 70, 083005
Bartolo N., Komatsu E., Matarrese S., Riotto A., 2004, Phys. Rep., 402, 103
Bartolo N., Matarrese S., Riotto A., 2005, J. Cosmology Astropart. Phys., 10, 10
Borgani S., Bonometto S. A., 1990, ApJ, 348, 398
Carbone C., Verde L., Matarrese S., 2008, ApJ, 684, L1
Cole S., Kaiser N., 1989, MNRAS, 231, 1127
Dalal N., Dore O., Huterer D., Shirokov A., 2007, Phys. Rev. D, 77, 123514
Desjacques V., 2008, MNRAS, 388, 638
Desjacques V., Seljak U., Iliev I. T., 2009, MNRAS, 396, 85
Efstathiou G., Frenk C. S., White S. D. M., Davis M., 1988, MNRAS, 235, 715
Eisenstein D. J., Hu W., 1999, ApJ, 511, 5
Gangui A., Lucchin F., Matarrese S., Mollerach S. 1994, ApJ, 430, 447

Gao L., Springel V., White S. D. M., 2005, MNRAS, 363, L66
Grinstein B., Wise M. B. 1986, ApJ, 310, 19
Grossi M., Dolag K., Branchini E., Matarrese S., Moscardini L., 2007, MNRAS, 382, 1261
Grossi M., Branchini E., Dolag K., Matarrese S., Moscardini L., 2008, MNRAS, 390, 438
Jenkins A., Frenk C. S., White S. D. M., Colberg J. M., Cole S., Evrard A. E., Couchman H. M. P., Yoshida N., 2001, MNRAS, 321, 372
Kaiser N., 1984, ApJ, 284, L9
Kang X., Norberg P., Silk J., 2007, MNRAS, 376, 343
Koyama K., Soda J., Taruya A., 1999, MNRAS, 310, 1111
Komatsu E., Spergel D. N., 2001, Phys. Rev. D, 63, 063002
Komatsu E. et al., 2009, ApJS, 180, 330
Lee J., Shandarin S. F., 1998, ApJ, 500, 14
LoVerde M., Miller A., Shandera S., Verde L., 2008, J. Cosmology Astropart. Phys., 04, 014
Lucchin F., Matarrese S., Vittorio N., 1988, ApJ, 330, L21
McDonald P., 2008, Phys. Rev. D, 78, 123519
Matarrese S., Verde L., 2008, ApJ, 677, L77 (MV08)
Matarrese S., Lucchin F., Bonometto S. A., 1986, ApJ, 310, L21
Matarrese S., Verde L., Jimenez R., 2000, ApJ, 541, L10
Mo H. J., White S. D. M., 1996, MNRAS, 282, 347
Mo H. J., Jing Y. P., White S. D. M., 1997, MNRAS, 284, 189
Pillepich A., Porciani C., Hahn O., 2008, preprint (arXiv:0811.4176)
Press W. H., Schechter P., 1974, ApJ, 187, 425
Reed D., Gardner J., Quinn T., Stadel J., Fardal M., Lake G., Governato F., 2003, MNRAS, 346, 565
Robertson B., Kravtsov A., Tinker J., Zentner A., 2008, preprint (arXiv:0812.3148)
Robinson J., Baker J. E., 2000, MNRAS, 311, 781
Robinson J., Gawiser E., Silk J., 2000, ApJ, 532, 1
Salopek D. S., Bond J. R., 1990, Phys. Rev. D, 42, 3936
Scoccimarro R., Sheth R., Hui L., Jain B., 2001, ApJ, 546, 20
Seljak U., 2008, preprint (arXiv:0807.1770)
Sheth R. K., 1998, MNRAS, 300, 1057
Sheth R. K., Tormen G., 1999, MNRAS, 308, 119
Sheth R. K., Tormen G., 2002, MNRAS, 329, 61
Sheth R. K., Mo H. J., Tormen G., 2001, MNRAS, 323, 1
Slosar A., Hirata C., Seljak U., Ho S., Padmanabhan N., 2008, 2008, J. Cosmology Astropart. Phys., 08, 031
Springel V., 2005, MNRAS, 364, 1105
Taruya A., Koyama K., Matsubara T., 2008, Phys. Rev. D, 78, 123534
Verde L., Wang L., Heavens A. F., Kamionkowski M., 2000, MNRAS, 313, 141
Verde L., Jimenez R., Kamionkowski M., Matarrese S., 2001, MNRAS, 325, 412
Viel M., Branchini E., Dolag K., Grossi M., Matarrese S., Moscardini L., 2009, MNRAS, 393, 774
Warren M. S., Abazajian K., Holz D. E., Teodoro L., 2006, ApJ, 646, 881
Yadav A. P. S., Komatsu E., Wandelt B. D., 2007, ApJ, 664, 680

APPENDIX A

We report here the explicit expression for the function $\alpha_M(k)$ which encloses the scale (and mass) dependence of the non-Gaussian halo bias. For a derivation of the expression from first principles, please see Matarrese & Verde (2008).

We start by defining the function $\mathcal{M}_R(k)$ which relates the Fourier transform of the smoothed linear overdensity field to the Fourier transform of the Bardeen potential:

$$\delta_R(\boldsymbol{k}) = \frac{2}{3}\frac{T(k)k^2}{H_0^2\Omega_{\mathrm{m},0}} W_R(k)\Phi(\boldsymbol{k}) \equiv \mathcal{M}_R(k)\Phi(\boldsymbol{k}) \,, \tag{A1}$$

where $T(k)$ denotes the matter transfer function and $W_R(k)$ is the Fourier transform of $W_R(\boldsymbol{r})$, the top-hat function of width R.

Then, we define the so-called 'form factor' $\mathcal{F}_R(k)$

$$\mathcal{F}_R(k) = \frac{1}{8\pi^2\sigma_R^2}\int dk_1 k_1^2 \mathcal{M}_R(k_1)P_\phi(k_1) \times \int_{-1}^{1} \mathrm{d}\mu \mathcal{M}_R\left(\sqrt{x}\right)\left[\frac{P_\phi\left(\sqrt{x}\right)}{P_\phi(k)} + 2\right], \tag{A2}$$

where P_ϕ denotes the power spectrum of the linear gravitational potential ϕ. The form factor is closely related to the primordial bispectrum, $x = k_1^2 + k^2 + 2k_1 k\mu$, and μ denotes the cosine of the angle between k_1 and k.

Finally $\alpha_M(k)$ is given by

$$\alpha_M(k) = \frac{\mathcal{F}_R(k)}{\mathcal{M}_R(k)} \,. \tag{A3}$$

Note that the mass dependence comes in only through the presence of the smoothing window W_R in $\mathcal{M}_R(k)$. For k-modes corresponding to scales larger than the Lagrangian radius of the haloes, $W_R = 1$. These are also the scales where the analytic derivation of the non-Gaussian halo bias effect holds, for example for a halo of mass $1 \times 10^{14}\,\mathrm{M}_\odot\,h^{-1}$ the comoving Lagrangian radius is $7\,\mathrm{Mpc}\,h^{-1}$ and $W_R(k)$ deviates significantly from 1 at $k \gtrsim 0.1\,h\,\mathrm{Mpc}^{-1}$. On scales $k \ll 0.1\,h\,\mathrm{Mpc}^{-1}$, $\Delta b/b$ shows no mass dependence.

It is useful to derive analytically an expression for $\alpha_M(k)$ valid on large scales. For the local type of non-Gaussianity, the bispectrum is dominated by squeezed configurations: in this limit, $\mathcal{F}_R(k)$ tends to unity for large scales where $W_R(k)$ goes to unity.

Therefore, on scales larger than the Lagrangian radius of the halo

$$\alpha_M(k) = \mathcal{M}_R^{-1}(k) = \frac{3}{2}\frac{H_0^2\Omega_{\mathrm{m},0}}{T(k)k^2} \sim \frac{H_0^2\Omega_{\mathrm{m},0}}{k^2}, \tag{A4}$$

where in the last step we have approximated the transfer function to unity on large scales. This last step offers a good approximation (to better that 20 per cent) on scales $k < 0.01\,h\,\mathrm{Mpc}^{-1}$.

This paper has been typeset from a TEX/LATEX file prepared by the author.